A Dissertation

Effect of Sintering Temperature on Structural, Conducting and Thermal Properties of Pyrochlore $Y_2Ti_2O_7$

Submitted By

Ms. MEENU

Roll No.600902015

in Partial Fulfillment of the Requirements for the Degree of

Master of Technology

in

Material and Metallurgical Engineering

Under Guidance of

Dr. KULVIR SINGH

School of Physics & Material Science

Thapar University Patiala Punjab, India 147004

(july-2011)

Acknowledgement

I am submitting my thesis report for the partial achievement of my M.Tech. degree. I express my deep gratitude and respect to my supervisor **Dr. Kulvir Singh, Associate Professor School of Physics and Material Science**, for his keen interest, strong motivation and constant encouragement during the course of the work. I thank him for his great patience, constructive criticism and numerous useful suggestions apart from invaluable guidance to me.

I would also like to thank Dr. O.P. Pandey, Professor and head of deptt, School of Physics and Material Science for his constant guidance and encouragement. I would like to thanks to Mrs. Jasmeet kour Gill who help me in my experimental work and unselfishly reading my thesis chapter and give valuable comment.

I would like to thanks to Mrs. Gurvinder Kour, Mr. Akshay Kumar, Mr. Ranveer Kumar, Mr. Gourav singla and Mr. Paramjyot Kumar Jha for their moral support and help whenever needed. I would like to convey my sincere gratitude to my friends and colleagues Mr. Suresh Kumar, Mr. Vipin Sharma, Mr. Ishvdeep Singh, Mr. Khushvendra Singh, Mr. Shrikant Verma and Ms. Richa Sharma for their support and their timely help and valuable discussions.

I owe my sincere thanks to all the staff members of School of Physics and Materials Science for their support and encouragement.

The meaning of my life and work is incomplete without paying regards to my respected parents whose blessings and continuous encouragement have shown me the path to achieve my goals. I would like to thank to my parents and my brothers for their patience, moral support and constant co-operation whenever I was away from them. And above all, I pay my regards to the almighty for his love and blessings.

Ms. MEENU

Certificate

This is to certify that this thesis entitled "**Effect of Sintering Temperature on Structural, Conducting and Thermal Properties of Pyrochlore $Y_2Ti_2O_7$**" which is being submitted by **Ms. MEENU** in fulfillment of the requirement for the award of degree of Master of Technology in school of physics and material science, Thapar university Patiala, Punjab is an exclusive record of candidate's own research under our supervision. The thesis in part or in full has not been submitted in any other university or in institute for the award of any degree. The thesis is fit to be considered for the award of degree of Master of Technology.

Dr. Kulvir Singh

Associate Professor

School of Physics and Material Science

Countersigned By:

Dr. O.P. Pandey

Professor & Head of Deptt.

School of Physics & Material Science

Dr. S. K. Mohapatra

Dean Academic Affairs

Thapar University Patiala Punjab

Abstract

Yttrium titanate $Y_2Ti_2O_7$, is isostructural with the mineral Pyrochlore. Samples have been prepared using high energy ball mill. Initial ingredients used in present study are TiO_2, Ti_2O_3 with Y_2O_3. Two type of samples YTi (TiO_2/Y_2O_3) and YTi2 (Ti_2O_3/Y_2O_3) are prepared. Pyrochlore phase $Y_2Ti_2O_7$ has been prepared by ball milling the initial ingredients upto 40 hours. Both samples have been sintered at 1450°C for 12 hours. It has been observed that YTi has Pyrochlore $Y_2Ti_2O_7$ phase whereas YTi2 has pyrochlore $Y_2Ti_2O_7$ and TiO_2 phase. Conductivity of YTi2 is found to be $2.23x10^{-6}$ S/cm which is an order higher than YTi. An exothermic peak has been observed at 850° C in both the samples. Lattice parameter of YTi and YTi2 are 9.90 Å and 9.97Å respectively. The relative density of YTi and YTi2 has been found to be 84% and 97% of theoretical density respectively. At high temperature range (T> 660°C); activation energy of YTi and YTi2 has been observed 0.61eV and 0.59eV respectively. Thermal expansion coefficient (TEC) of YTi and YTi2 has been found to be $8.389x10^{-6}$/K and $8.212x10^{-6}$/K respectively.

During the second part our study we sintered both samples pellet at 800°C and 1000°C for 12 hours. Concentration of TiO_2 in YTi2 sample is found to be higher than single sintered YTi 2. Conductivity of both double sintered samples is of the same order (~$2.99x10^{-4}$ S/cm) and greater than the conductivity single sintered sample. No exothermic peak was observed in differential thermal analysis. Density of double sintered samples is comparatively very low than single sintered samples. Lattice parameter of YTi and YTi2 is found to be 10.15Å and 10.02Å respectively. Thermal expansion coefficient (TEC) of YTi and YTi2 is found to be $8.343x10^{-6}$ /K and $8.405x10^{-6}$ /K respectively. Due to lower density of double sintered samples, activation energy is low in comparison of single sintered samples.

Contents **Pages**

List of Figure

List of Tables

Chapter-1 Introduction

This chapter presents a review of ionic conductor. The mechanism of ionic conduction which is key property of solid electrolyte. Defect formations that govern origin of ionic conductivity have been discussed. Structure of the various oxygen ion conductors like pyrochlore [1] which play important role for ionic conductivity enhancement is also discussed. In addition to this processing technique of pyrochlore is also discussed.

1.1 Introduction to ion conduction in solid state

Many solids exhibits high ionic conductivity ($>10^{-4}$ Scm^{-1}) and they are of immense use in diverse technological applications. Some of these solids which are also good electronic conductors are often referred to as 'mixed conductors', while the term 'super ionic conductor' or 'fast ion conductor' is reserved for good ionic conductors with negligible electronic conductivity. One of the most important use of super ionic conductors are, electrolytes in battery applications and hence, often, they are referred to as 'solid electrolytes' as well. There are many advantages in electrochemical devices using solid electrolytes instead of liquid electrolytes. These include, among others, longer life, high energy density, no possibility of leak etc., and are particularly suitable in compact power batteries used in pace-makers, mobile telephones, laptops etc. Mixed ion conductors find application in electrochemical devices as electrode materials.

1.2 Ionic vs. Electronic Conductivity

There is a comparison between the properties of ionic conductors with the conventional electronic conductors such as metals.

Metals

1. Conductivity Range = 10 S/cm to 10^5 S/cm
2. Electrons carry the current
3. Conductivity Increases linearly as temperature decreases (phonon scattering decreases as T ↓)

Solid Electrolytes

1. Conductivity Range = 10^{-3} S/cm to 10 S/cm
2. Ions carry the current
3. Conductivity decreases exponentially as temperature decreases (activated transport)

1.3 Conduction mechanisms

For ionic conductivity, transport of one or more types of ions across the material is necessary. In an ideal crystal all constituent ions are arranged in regular periodic fashion and are often stacked in a close-packed form. Thus, there is little space for an ion to diffuse. Often, the available space is just enough for vibration around its equilibrium position. However, at any non-zero temperature there exist defects. These could, for example, be positional disorder due to deviation from ideal stacking. The degree of such disorder can vary from one material to another or even from one temperature or pressure to another in the same material. At zero temperature, the free energy is dominated by the potential energy. Hence the arrangement of ions in an ideal crystal at zero temperature is such that the total potential energy of the system is the lowest. As the

temperature of the system increases, the contributions to free energy from entropy become more and more prominent. The entropy, as it is often described, is a measure of the degree of disorder. Thus the origin of the crystal defect arises from the system attempting to minimize the free energy through an increase in the entropy.

1.4 Role of Defects

In order to move an ion through a crystal it must hop from an occupied site to a vacant site. Thus ionic conductivity can only occur if defects are present. Two types of defects important in the context of ion mobility in crystals are 'Schottky' and 'Frenkel' defect. These belong to the class of 'point defects' in crystals. If imperfections in the crystal are such that the ratio between the anions and cations remain same as represented by the molecular formula, the defect is called a stoichiometric defect. These two stoichiometric defects are as follows:

- Schottky defect
- Frenkel defect

1.4.1 Schottky Defect

In an ionic crystal of the type $A^+ B^-$, equal number of anions and cations are missing from the lattice sites so that electrical neutrality is maintained it is called schottky defect. In general schottky defects are present in 10^{16} ions in annealed ionic solids.

This type of defect is shown by highly ionic compounds which have

- High coordination number
- Cations and anions of similar sizes.

Examples: KCl, NaCl, KBr and CsCl.

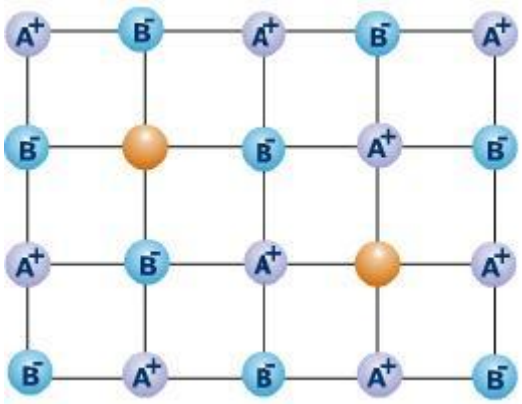

Fig 1.1 (a) - Schottky defect in ionic solids.

Consequences of Schottky Defect:

- As the number of ions decrease, volume is the same, so density decreases.
- Crystals with Schottky defect conduct electricity to a small extent.
- Due to the presence of holes the stability of the crystal decreases.

1.4.2 Frenkel Defect

If an ion is missing from its lattice site (causing a vacancy or a hole there) and it occupies the interstitial site so that electrical neutrality as well as stoichiometry of the compound are maintained. This type of defect is called Frenkel defect as shown in fig.1.1 (b). Since the sizes of cations are generally smaller it is more likely that cations occupy interstitial sites. This type of defect is present in those compounds which have

- Low co-ordination number.
- Large difference in size of anion and cation.

  Examples: AgCl, AgBr, AgI and ZnS.

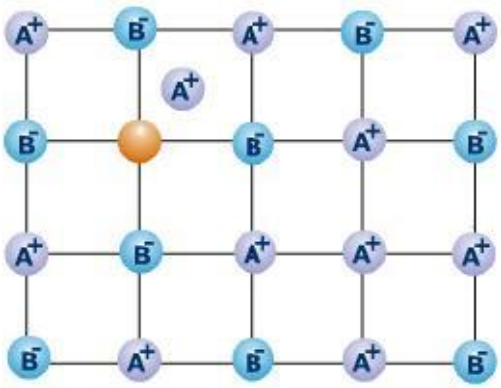

Fig 1.1 (b) - Frenkel defect in ionic solids.

Types of compounds exhibiting Frenkel defect

Consequences of Frankel Defect:

- Solids with this defect conduct electricity to a small extent
- The dielectric constant of the crystal increases
- The density of the solid is unchanged
- Due to the presence of holes, the stability of the crystal decreases.

1.5 Fluorite structure

The term "fluorite" originates with the mineral CaF_2, which is generally known by the same name. Oxides which adopt the fluorite structure or structures related to fluorite have great and varied technological importance. The fluorite structure is AO_2. This structure is a face centered cubic arrangement of cations with anion occupying all the tetrahedral sites as shown in fig. 1.2. Fluorite structure has large number of octahedral interstitial voids. UO_2, ThO_2. CeO_2 are materials that readily form the fluorite structure. Despite the vast difference in applications, the crystal structures of fluorite and pyrochlore compounds are very similar. In following figure small circle represent Ca^{+2} and big circle represent F^{-1}.

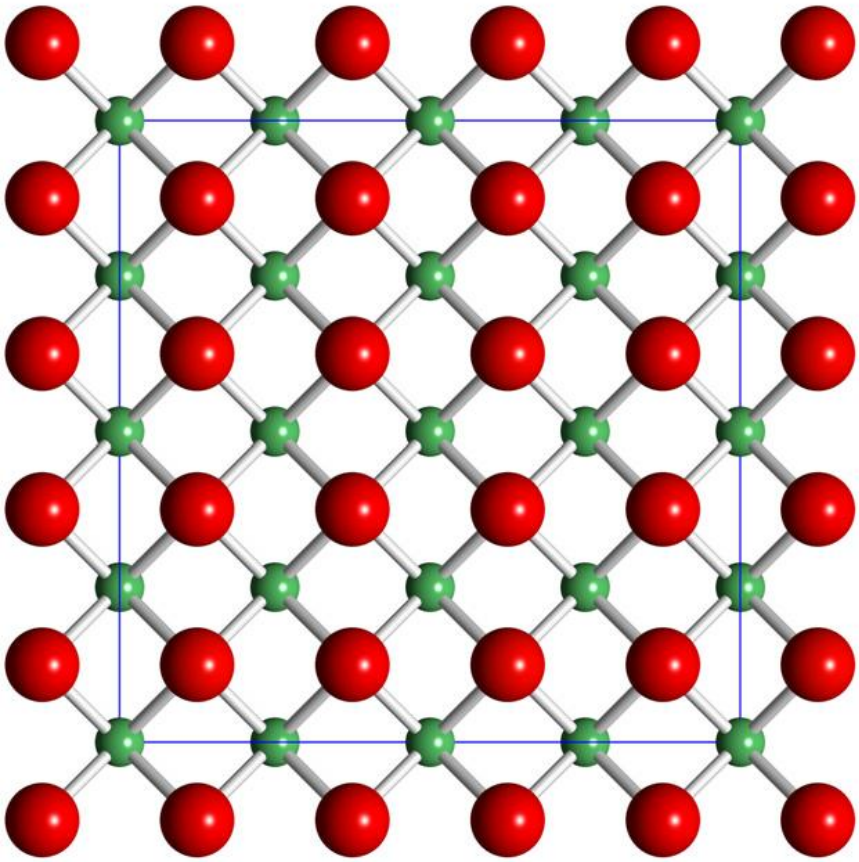

Fig-1.2**:** Schematic Diagram of Fluorite structure.

1.6 Pyrochlores Structure

Pyrochlore is the name given to naturally occurring mineral discovered by Woehler, having the formula $A_2B_2O_7$. In Greek, “pyro” means fire and “khloros” means green. Pyrochlore turns green on heating. Pyrochlore structure is super derivative of Fluorite structure. Stoichiometry of ideal pyrochlore will be $A_2B_2X_6X'$. A is larger cation and B is smaller one. A is a trivalent rare earth ion, but can also be a mono, divalent cation and B may be 3d, 4d or 5d transition element having appropriate oxidation state required for charge balance to give rise to composition $A_2B_2O_7$ as

shown in fig-1.3. The Pyrochlore Structure (1/8 unit cell). Large blue spheres are A^{3+} ions, small red spheres are B^{4+} ions, and larger yellow spheres are O^{2-} ions**.**

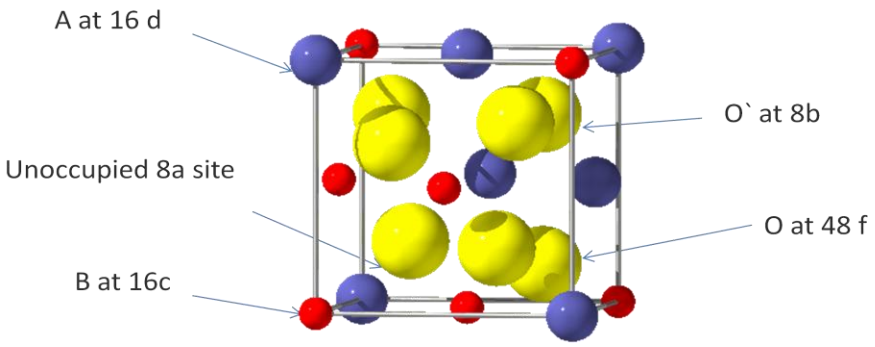

Figure 1.3: Schematic Diagram of Pyrochlore structure.

1.6.1 Ordered Pyrochlore Structure

Pyrochlore structure is cubic with space group Fd-3m, Z=8, with general formula $A_2B_2O_6O'$. A Cation forms fcc array and 1/8 of anions are removed to maintain charge neutrality. These oxygen vacancies are ordered and A and B are alternated in <110> rows, resulting in doubling of fluorite lattice parameter (Fd-3m, Z=4) [1]. There are five crystallographic position which are available at various site: 16d for A cation, 16c for B cation, 48f for O, 8b for O' whereas 8a site (1/8,1/8,1/8) is vacant [2]. Oxygen anion at 8b site, is at undisturbed position (3/8, 3/8,3/8) with

respect to the fluorite structure and tetrahedrally coordinated by A cations. While oxygen anion at 48f (x,1/8,1/8) are displaced towards the neighboring vacant 8a sites and are bounded to two A and two B cation. The A cation occupy an axially compressed scalenohedron coordinated by 6 O (8b) and two O` (48f) atoms. Hence A-O and B-O length depend upon the lattice parameter and oxygen position [3,4,5].

1.6.2 Disordered Pyrochlore Structure

Pyrochlore is a oxide in which order-disorder transformation take place in anion and cation array in the structure. X-ray diffraction pattern detect the disorderness at the oxygen site. The size difference between cation and anion species that occupy the A and B is believed to be driven force for ordering in pyrochlore structure. Disorder evolves at independent rate in cation and anion array despite Coulumbic-interaction between them. Occupation of 8b oxygen site associated with the disorder on the cation site [6]. Disordering of cation site coupled with oxygen disorder on the anion vacancies within the pyrochlore structure result in defect fluorite structure. Disordering induce ionic radii difference in cation A and B sites. The change in ionic radii enhances the formation of anion Frankel defect which lead to high ionic conductivity in pyrochlore material [2, 3].

1.7 Doping Phenomena in Pyrochlore Systems

Two types of pyrochlores of these forms are available: $(A^{3+})_2(B^{4+})_2X_6X'$ (III, IV-pyrochlores); $(A^{2+})_2(B^{5+})_2X_6X'$(II, V-pyrochlores). In these structures A-sites are occupied by large, low oxidation state cations such as lanthanide ions, Y, Bi, In, Tl, Pb(II), Sc, Cd, Hf, Hg(II), Ca, Sr, Mn(II), Sn(II) etc. X, X' anions could be O^{2-} , F^-, OH^-, N^{3-}. It is formed when 1/8 of the oxygen atom is removed from ideal fluorite structure. The additional anion vacancy resides in the tetrahedral interstice between adjacent B-site cations. For an ideal pyrochlore structure the r_A/r_B

ratio should be in the range of 1.45-1.8. These systems are particularly susceptible to geometrical frustration and novel magnetic effects. The B-site ions are octahedrally coordinated by X ions and A-site ions having distorted cubic coordination by X and X'. X-site ions are tetrahedrally coordinated by 2 A and 2 B ions while X'- site ions are tetrahedrally coordinated by 4 A ions. Fig 1.4 shows the doping in pyrochlore system. The largered spheres are oxygen, the green (La/Y) and blue (Zr/Hf) smaller spheres are the cations. Small black spheres indicate the unoccupied 8b position.

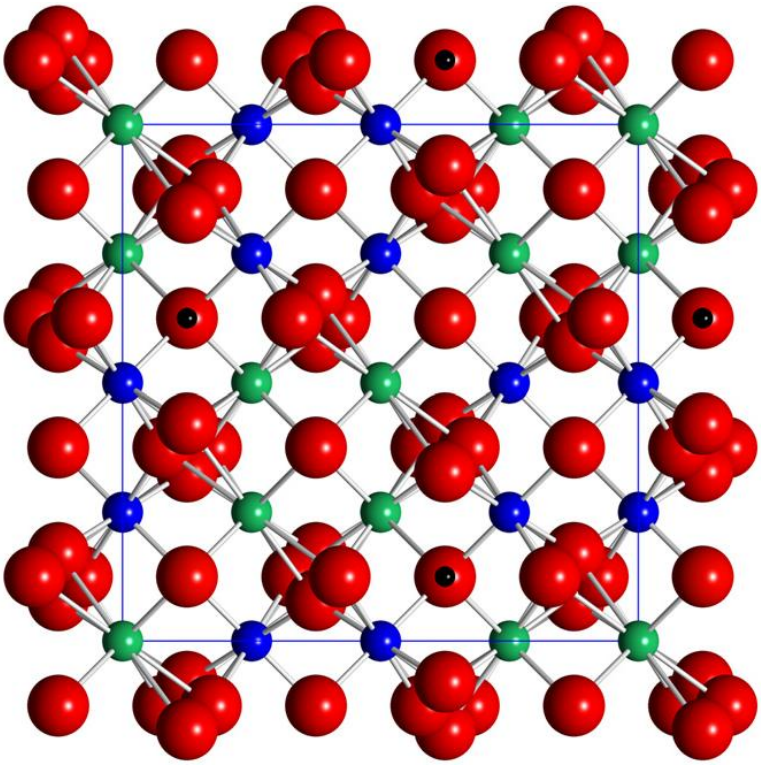

Figure 1.4: This shows the doping in pyrochlore system.

1.8 Properties of pyrochlore

A large number of pyrochlore such as $Y_2Nb_2O_7$, $Y_2Zr_2O_7$ and $Gd_2Zr_2O_7$ etc. have been synthesized with an amazing variety of chemical composition and exploitable properties [7-10]. The pyrochlore structure shows varied physical properties ranging from electronic insulators [11] $La_2Zr_2O_7$, ionic conductors [12] $Gd_{1.9}Ca_{0.1}Ti_2O_{6.9}$, metallic conductivity, $Bi_2Ru_2O_{7-y}$, Mixed Ionic and Electronic Conductivity [13], spin ice systems $Dy_2Ti_2O_7$, spin glass systems $Y_2Mo_2O_7$ [14] and superconducting materials [15] $Cd_2Re_2O_7$. Pyrochlore oxides have been proposed as matrices for immobilizing high level radioactive waste [16]. Some of the very important properties of the members of the pyrochlore group are low thermal conductivity, high melting point, high thermal expansion coefficient and high stability.

1.9 Application of Pyrochlore

Synthetic pyrochlore has a great variety of chemical compositions due to substitutions at the A and B sites. Over 450 synthetic pyrochlores have been synthesized with this structure type [17].

1. They can be used in gas turbines and diesel engines as thermal barrier coatings. In aircraft turbines, ceramic coatings on turbine blades with low thermal conductivity and high emittance are used for thermal insulation of the metallic components, which allows a higher gas temperature and finally leads agreeable to higher energy efficiency.
2. Some of the pyrochlore compounds exhibit high ionic conductivity and can be used as electrodes for fuel cells.
3. Pyrochlore oxides also exhibit catalytic properties and are used as solid photo catalysts, oxidation catalysts and gas monitoring sensors.
4. They have the ability to accommodate defects and act as possible host for radioactive wastes and as host for fluorescence centers.

5. Some of the pyrochlore materials also show superconductivity and magnetic properties including colossal magneto resistant behavior.
6. Radiation effects in pyrochlore-based titanate ceramics have been extensively studied[18,19]
7. Communication/Portable Electronics Mobile phones/Notebook PCs: Li-ion batteries using gel electrolytes and mixed conductors.
8. Micro-batteries for Smart Cards/Micro-electro-mechanical devices.
9. (MEMS): Li-metal or Li-ion batteries using Li-solid electrolytes
10. Display devices Electrochromic displays: H^+ or Li^+ conductors as solid electrolytes.
11. Medicine Li batteries for implantable pacemakers: in large-scale use for many years.
12. Oxygen sensors for analyzing the exhaust gases to control the combustion process for environment protection and fuel saving purposes: Large-scale application in both the automotive industry and power plants.

1.10 Mechanical Alloying

Pyrochlore can be synthesized by different techniques such as solid state reaction method, chemical route, co precipitation method and thermo mechanical methods. In the following section thermo mechanical method will be discussed. High energy ball milling (mechanical alloying) induces high energy impact on charge powder by collision between balls and particle causing plastic deformation, repeated fracturing and cold working of particle leading to nano crystalline materials [20,21]. The mechanical alloying techniques allow alloying of elements that are difficult or impossible to combine by conventional melting methods due to high vapour-pressure or large difference in melting temperature of components. Moreover in Mechanical alloying (MA) the process is carried out at room temperature [22,23] Basically, the process can

be viewed as a means of assembling metal constituents with a controlled microstructure. If two metals will form a solid solution, mechanical alloying can be used to achieve this state without the need for a high- temperature excursion. Conversely, if the two metals are insoluble in the liquid or solid state, an extremely fine dispersion of one of the metals in the other can be accomplished. The process of mechanical alloying was originally developed as a means of overcoming the disadvantages associated with using powder metallurgy to alloy elements that are difficult to combine.

Some oxides are insoluble in molten metal. Mechanical alloying provides a means of dispersing these oxides in the metals. For example nickel-based super alloys strengthened with dispersed thorium oxide or yttrium oxide (Y_2O_3). These super alloys have excellent strength and corrosion resistance at elevated temperatures, making them attractive candidate materials for use in applications such as jet-engine turbine blades, vanes, and combustors. Many other potential applications for mechanical alloying material are being explored, including powders for coating applications, alloys of immiscible systems, amorphous alloys, intermetallics, cermets, and organic-ceramic-metallic material systems.

Mechanical alloying (MA) is a high energy ball milling process to develope materials with homogeneous microstructure and novel properties from the elemental blends. Mechanical alloying is known to lead to the formation of a variety of stable and metastable phases depending on the alloy system and MA conditions studied. Mechanical alloying has been shown in the literature as a viable route for the synthesis of intermetallics with high melting points, which are difficult to form by a conventional metallurgy route. In addition, these intermetallics can be synthesized in nanocrystalline form by mechanical alloying, which potentially leads to improvement in their properties.

Microstructural refinement to a nanometer level is expected to increase both the strength and ductility of intermetallics, which can be achieved easily at room temperature by mechanical alloying. In addition, nanocomposites developed with nanocrystalline intermetallics embedded are reported to have enhanced mechanical properties, which have been reported to develop by non-equilibrium processing routes like mechanical alloying and rapid solidification processing (RSP). Following figure shows the mechanical alloying of material by using ball mill.

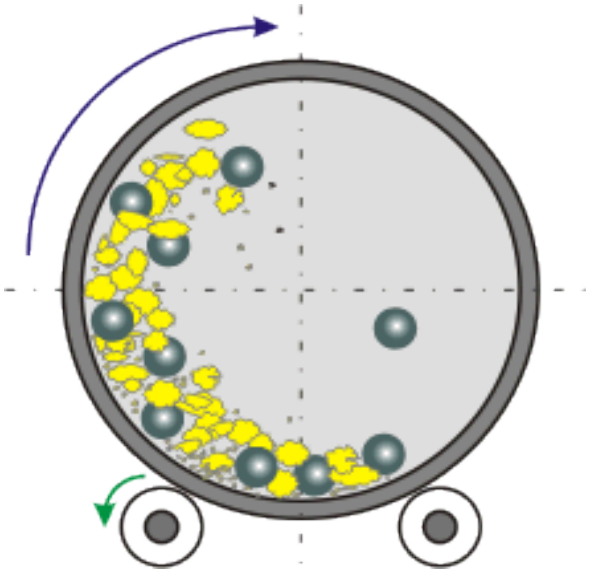

Figure-1.5- Ball milling: mechanical alloying.

Chapter-2 Literature Review

This chapter introduces literature review on pyrochlore oxide and its various properties. Here we also focus on result which was obtained by processing of pyrochlore, by using mechanical alloying and effect of mechanical alloying on pyrochlore oxides properties.

Antonio et al. [24] were synthesized disordered pyrochlore, $A_2B_2O_7$ by mechanical milling of constituent oxide and successfully prepared at room temperature. They obtain result and suggest that mechanically activated chemical reaction between A_2O_3 (A=Y, Dy and Gy) and TiO_2, involve an initial step of particle and crystalline size reduction of constituent oxides together with the polymorphic transformation of the trivalent element oxides, from cubic into monoclinic A_2O_3. Formation of highly disordered pyrochlore, $A_2B_2O_7$ seem to take place as second step.

Hanawa et al. [25] found that superconducting pyrochlore oxide $Cd_2Re_2O_7$ exhibit a novel structure phase transition at ~ 73˚C from an ideal cubic structure to another cubic structure on cooling i.e. large change in structure produce large change in resistivity and magnetic properties. They investigate the relation in crystal structure and electronic structure in pyrochlore.

Zhi-fen fu et al. [26] synthesized $Mg_4Nb_2O_7$ nanopowder by using high energy ball milling and observed that crystallization and reaction are enhanced with increasing the milling time.

Diaz-Guillen et al. [27] found that La substitution for Gd in pyrochlore-type $Gd_2Zr_2O_7$ does not affect its ionic conductivity at least for $Y<0.8$, Despite of decreasing number of mobile oxygen. They conclude that reduction of ion-ion interactions promoted by more ordered

structure in sample with higher La-content.

Lee et al. [28] investigated electrical conductivity of Nb_2O_5 system. They focused on the relationship between the ionic conductivity and the existing phases. The isothermal ionic

conductivity in-creased as the value of x increased in the range of 2.5–20, which corresponds to the increase in the fraction of Fluorite F-phase in the crystal field (C+F) two-phase region. The decrease of isothermal ionic conductivity of the 20–25 and 27–50 mol% Nb_2O_5 compositions was probably due to the decrease in the oxygen-vacancy concentration. The 20 mol% Nb_2O_5 sample exhibited the highest conductivity and a very wide range of ionic domain, up to very wide range of pressure.

Gregory et al. [29] proposed that large decrease (nearly 527˚C) in measured Tc of the YTS pyrochlore series with increasing Sn content, for ion irradiation with 1.0MeV Kr ions, appears to be largely due to differences in the combined anion-Frenkel and cation-antisite disorder energy. In other words the specimen with x = 1.6 appears to disorder to the defect fluorite sub cell at a low fluency and then remains crystalline up to a fluence of 5 to 15 ions cm^{-2} upon irradiation at 50 K. Ion irradiation experiments for selected NTZ and LYH samples indicate that the energetic of cation/anion disorder also play a major role in determining the radiation response of these pyrochlore compounds. Chemical bonding, based on the Pauling electro negativity scale, only has a minor effect on radiation tolerance in the YTS and NTZ pyrochlores. At present, no compelling evidence found to suggest that Tc in the YTS system is nonlinear in composition (the same conclusion applies to the GTZ system). Collectively, the observed Tc values of pyrochlores in all three systems reported in this paper are essentially linear in r_A/r_B and x(48f), giving threshold values of these parameters below or above which the thin crystals remain crystalline during irradiation with 1.0MeV Kr ions respectively. Furthermore, some of the data fall within previously unexplored regions of the A-B cation radius space for III-IV pyrochlores, suggesting that the data may be useful for future refinement of the empirical models. This effort should

include studies of pyrochlore compounds with B = Ru and Mo as well as other ternary pyrochlore compounds.

Hayward et al. [30] explained the low-temperature top tactic reduction of $Y_2Ti_2O_7$ with calcium hydride which yields a mixture of two reduced pyrochlore phases ($Y_2Ti_2O_{6.5}$) and $Y_2Ti_2O_{5.9}$) which bound a region of unstable composition ($Y_2Ti_2O_7$.x, 0.5 x 1.1). Magnetic susceptibility data are consistent with metallic delocalized behavior in these phases. Such behavior suggests that phases of the form $Y_2Ti_2O_7$.x are unlikely to be good model systems for the study of geometrically frustrated magnetism.

Muthukkumaran et al. [31] have summarized and predicted the connection between defect association and ionic conductivity directly from quantum mechanical calculations. The site preference of vacancies is also determined depending upon their elastic and electronic interaction with the trivalent dopants and it is found that for atomic number close to 61 and 62 the elastic and electronic interaction are balanced and total interaction in the NN and NNN position are almost identical. The minimum activation energy (Ea), which decides the low barrier migration paths and in turn the ionic conductivity, when the E_f is independent of local atomic configuration and this happens for atomic number close to 61 and 62. We conclude here that pm3+ and Sm3+are best dopants for achieving high ionic conductivity. It is also suggested that a mixture of 3+ ions which results in atomic number between 61 and 62 may lead to a higher ionic conductivity than if any of them is used as a single dopant.

Shin et al. [32] proposed that in $Lu_2V_2O_7$, the orbital ordering, which extends toward the center-of-mass of the V tetrahedron, produces the ferromagnetic state due to the energy gain through the hopping process from t_{2g} orbital to e_g orbital. For this material, the interaction can be estimated

through the comparison between our calculation and inelastic neutron scattering. Thus, comparison with the inelastic neutron scattering experiments are strongly desired. Especially, the nature of the low-lying excitation strongly depends on the local uniaxial anisotropy. From the low-lying excitation and the polarized direction of the ferromagnetism, we can check the existence of the uniaxial anisotropy.

Malkin et al. [33] measured temperature-dependent absorption spectra of $Yb_2Ti_2O_7$ single crystals and emission and excitation spectra of $Y_2Ti_2O_7$:Yb (1%) polycrystalline samples. The energies of all the crystal-field levels within the 4f 13 configuration of Yb^{3+} in titanates with the pyrochlore structure have been found from the analysis of the spectra. They have performed the crystal-field calculations, starting from the model calculations in the framework of the exchange-charge model, and obtained the set of CF parameters that describes satisfactory the optical spectra observed in this work as well as experimental data obtained earlier on magnetic g factors and the temperature dependence of the electric-field gradient at the Yb3+ nucleus. Starting from the CF parameters for $Yb_2Ti_2O_7$, we obtained the sets of CF parameters for different other $R_2Ti_2O_7$ compounds and used them to calculate CF energies and g factors. A comparison between the calculated and experimental values (known from earlier works) always revealed good agreement. This gave us a possibility to analyze the trends in the variation of CF parameters along the series of R titanates with pyrochlore structure. Unusual stability of the BO_2, BO_4, and BO_6 parameters has been explained by considering the role of nonequivalent O_1 and O_2 oxygen legends.

Park et al. [34] evaluate the bulk densities of the sintered specimens were in the range of 5.42–5.63 g/cm^3, which was 94–97% of the theoretical density of ZnO 5.78 g/cm3.The density decreased with increasing Y_2O_3 content. Most of the added Y_2O_3 were segregated at nodal points

and grain boundaries, and found to form Y-rich phase together with Pr-rich phase. The average grain size decreased with increasing Y_2O_3 content and decreasing sintering temperature. The barrister voltage and the nonlinear coefficient (α) increased as the amount of Y_2O_3 content was increased. The dielectric constant (ε) decreased with increasing Y_2O_3 content. The specimen with 4.0 mol% Y_2O_3 sintered at 1285°C exhibited the highest nonlinearity, with a nonlinear coefficient of 77, and the dielectric constant 352 at 1 kHz.

Johnson et al. [35] evaluated the molecular dynamics simulations of the thermal conductivity of $Y_2Ti_2O_7$ at T ¼ 1473 K predict a value of 2.6W $m^{-1}K^{-1}$, not unreasonable in light of the present results. From the perspective of thermal barrier coatings, pyrochlores are thought to be competitive as replacements for yttria-stabilized zirconia, especially if the thermal conductivity can be lower than 2–3W $m^{-1}K^{-1}$. Our results are for a single crystal of highly purified $Y_2Ti_2O_7$so the values of k are maximal, and polycrystallinity, porosity and addition of impurities could lower the thermal conductivity into a useful range for thermal barrier coatings. Pyrochlores have been suggested as an inert matrix for actinide transmutation and to efficiently remove heat from matrices with high concentrations of actinides, k in the range above ca. 2W $m^{-1}K^{-1}$ is required. Compared with $Nd_2Zr_2O_7$ and $La_2Zr_2O_7$ (1.7W $m^{-1}K^{-1}$ and 1.5W $m^{-1}K^{-1}$, our data show that $Y_2Ti_2O_7$ also holds promise for these applications.

Chartier et al. [36] proposed that oxygen atoms play little role in the order-disorder transitions because the cation order parameter drives that of the oxygen atoms. Accumulation of FPs is the mechanism that drives zirconium pyrochlores towards amorphization following a two-step process: First, a transition from pyrochlore to disordered fluorite that occurs for about a 0.2 FP per cation ratio in $La_2Zr_2O_7$. Second, subsequent irradiation produces more FPs, and the amorphization of disordered fluorite $La_2Zr_2O_7$ takes place for a critical FP concentration of 0.1.

In the low temperature limit a total number of 0:2, 0:1, 0:3 FPs per cation should be produce by irradiation to fully amorphize lanthanum zirconate pyrochlore. The amorphization thus relies on the ability to reach a significantly high critical FP concentration before the crystalline structure collapses. This mechanism provides atomic-level interpretation of the difficulty to amorphize lanthanum zirconate, as evidenced by its low critical temperature of 310 K. As soon as the temperature is large enough to activate the diffusion of cation vacancies or interstitials, recombination takes place, and it becomes impossible to reach the critical concentration. Such diffusive recombination processes may prevent the amorphization of the other zirconate pyrochlores.

Deepa et al. [37] prepared a new series of semiconducting oxides in Ca–Ce–Ti–M–O (M = Nb or Ta) system and its structural, micro structural and electrical conductivity properties were investigated. The powder X-ray diffraction and Raman spectroscopy analysis showed that all these compounds belong to a cubic pyrochlore type structure in the space group Fd-3m. The Semi conductivity in these compounds is due to the presence of Ce^{3+}, which remains in the reduced state without being oxidized to Ce^{4+} by structural stabilization. The presence of Ce^{3+} is further confirmed by the X-ray photoelectron spectroscopy and photoluminescence studies. Impedance spectral studies suggest that the conduction in these compounds is mainly due to electronic contribution. Among the prepared compounds, $(Ca_{0.75}CeTi_{0.25})(Ti_{1.5}M_{0.5})O_7$ (M = Nb or Ta) possesses good NTC behavior over a wide temperature range. Therefore, these semiconducting ceramic oxides may find potential applications in devices like NTC thermistors and further work is in progress in this line.

Whittle et al. [38] explained the addition of a fluorite driver such as Y^{3+} in place of La^{3+} in pyrochlores containing Zr or Hf on the B site ultimately removes the superstructure and the

compositional limit for a single phase fluorite is$1.4<x<1.6$ in the $La_{2-x}Y_xZr_2O_7$ series and for $1.6<x<2.0$ in the $La_{2-x}Y_xHf_2O_7$ series. The main two-phase region in the Hf-based pyrochlores is shifted to a much higher level of Y^{3+} doping than in the Zr-based series, close to x = 1.2 in these slowly cooled samples. For the same level of Y doping, the Hf samples are also more pyrochlore-like with regard to the systematically larger x-coordinate of the 48f oxygen position. TEM investigations illustrate that the defect fluorite phase exhibits evidence of short-range correlations in both systems, with the modulated structure being somewhat more ordered(pyrochlore-like) in the Hf-based samples. These results suggest that as a waste form pyrochlore based materials are ideal for elements such as U^{4+} and Pu^{4+}, which are both fluorite drivers.

Tan et al. [39] explained with careful attention to the Rietveld refinement procedure, and by testing the validity of possible models containing different site multiplicities, parameters and occupancies, satisfactory models for the average structures of the present pyrochlore phases are obtained. It is clear that the different-sized Zn^{2+} and Bi^{3+} ions occupy different positions within the A-sites. This is linked to off centre displacement of surrounding O(2) ions, allowing a local structure (presently undefined) that gives reasonable Zn–O and Bi–O bond lengths. Oxygen non-stoichiometry, associated with variable cation contents in the pyrochlore solid solutions, is readily accommodated by partial occupancy of O(2) and O(3) sites, which occurs even in the case of the stoichiometric composition, $Bi_{1.5}ZnTa_{1.5}O_7$. Variable cation stoichiometry is accommodated by varying the X: Zn occupancies of the B-sites together with the Bi: Zn occupancies of the A-sites, but without any evidence for spillover of either excess Bi onto the B-sites or excess X onto the A-sites. There is some evidence that Zn deficiency is accommodated by B-site vacancies. Off-centre displacement of both A-site ions (to different off-centre sites for

X= Nb, Ta) and O(2) ions provides a mechanism for satisfying the bonding requirements of the different-sized Bi^{3+} and Zn^{2+} ions. The flexibility in cation and oxygen (O(2) and O(3)) site distributions and occupancies provides a basis to rationalize the unusual solid solution ranges that are found and that are significantly different for X= Nb, Ta and Sb.

Mandal et al. [40] prepared a series of compounds with the nominal compositions $Nd_{2-y}Y_yZr_2O_7$ ($0.0 \leq y \leq 2.0$) by solid state route. The continuous decrease in the lattice parameter with increase in Y^{3+} content till y=0.8 in the series proves the homogeneity range till that compositions. With increase inY^{3+} content in the system, the distinction between A and B sites diminishes which further leads to anti site defects formation which results into local oxygen disorder as evidenced by increased width of the Raman modes. The next two compositions, i.e. y =1.2 and1.6 are found to be biphasic in nature. The x parameter of 48f oxygen of compositions with pyrochlore structure shifts from 0.330(1) for $Nd_2Zr_2O_7$ to 0.345(6) for $Nd_{0.8}Y_{1.2}Zr_2O_7$, which is clear indication of increase in disorder in the system. One more significant conclusion can be drawn that variation at A site can also leads to order–disorder transition which supports the theoretical predication of Lian et al. [27]. Interestingly, Raman spectroscopy substantiated the result obtained from XRD data analysis. All the Raman peaks could be assigned properly. Moreover, this study revealed that 48f oxygen is involved in anionic disorder.

H.Du et al. [41] prepared Pyrochlore-type quaternary systems with the generic formula. $Bi_{1.5}Zn_{0.5}/.Nb_{0.5}M_{1.5}/O_7$ (M = Ti, Sn, Zr, and Ce) having a density higher than 95% of the theoretical density by a conventional ceramic solid-state reaction method. Positron annihilation lifetime techniques have been performed to identify the structural defects in the samples. The bigger difference of the weighted ionic radius r_w of the B-site, the higher the positron lifetime τ_{ave} value, corresponding to more grain boundaries and defects in BZNM. As the concentration

of the complex defect is enhanced, the concentration of free vacancies is decreased quickly because of defect accumulation. When bigger radius ions (Zr^{4+} and Ce^{4+}) are induced into BZN compounds, BO_6 octahedron distortion occurs, causing an increase of complex-defect concentration in the compounds, resulting in an increase in τ_2 and a decrease in I_2. The electrical study showed that weakly bonded electrons are reckoned to be the main charge carriers in the low-temperature range, and it is difficult to make oxygen ions the charge carriers. But when it comes to the high-temperature range, oxygen vacancy transference becomes active as the charge carrier mechanism. As there are the most structure defects in the BZNCe sample, there should be the greatest oxygen ionic conduction contributing to the total conductivity σ of this material, leading to the σ value being the largest of the four samples.

Ding et al. [42] fabricated $Y_2Ti_2O_7$ ceramics doped separately with 1 mol.% of rare earth oxides La_2O_3, CeO_2, Nd_2O_3, Sm_2O_3, Eu_2O_3, Gd_2O_3 and Dy_2O_3 by the conventional mixed oxide method. The results demonstrated that the ceramics exhibited cubic pyrochlore $Y_2Ti_2O_7$ as main phase and well crystallized at 1450 ºC. It was obvious that proper rare earth ions into $Y_2Ti_2O_7$-based ceramics could bring down the dielectric loss greatly, and made τ_f tend to zero. The $Y_2Ti_2O_7$ ceramics doped with 1% Nd_2O_3 exhibited optimum microwave dielectric characteristics: $\varepsilon r \approx 45$, $Q \cdot f \approx 22000$ GHz, $\tau f = 179$ ppm/ºC. The material could be used as resonators and filters applying in 3–8 GHz of microwave spectrum.

Belov et al. [43] prepared $(Ln_{1-x}A_x)_2Ti_2O_7-\delta$ (Ln = Dy, Ho; A = Ca, Mg, Zn; x = 0–0.1) pyrochlore solid solutions first time using mechanical activation, co-precipitation and solid-state reactions. The conductivity of the ceramics prepared via co-precipitation and from mechanically activated oxides exceeds that of the samples prepared by solid-state reactions at the same temperature, owing to a more even dopant distribution over the ceramic grains. The solid-state

method can, in principle, provide the close doping distribution but only at the higher synthesis temperatures. However the grain-boundary conductivity component is seen to have non-Arrhenius behavior in the samples synthesized by solid-state method. The activation energy for conduction depends little on the sample composition and preparation procedure, with a tendency to rise upon A^{2+} substitution for Ln^{3+}.

Radhakrishnan et al. [44] determined the structural variation, Pyrochlore to Fluorite type in the solid solutions of different ratios: 4:1, 2:1, 1:1, 1:2, 1:4, 1:6 of $CaTaO_{3.5}$ and $YZrTaO_{3.5}$. The pyrochlore phase stabilizes for the r_A/r_B 1.69–1.57 and the defect fluorite phase for 1.47–1.45 values. The structural disorder induced in the present system for r_A/r_B =1.47 as the ratios of the solid solutions of $CaTaO_{3.5}$ and $YZrTaO_{3.5}$ were changed from 4:1 to1:4. This ratio, r_A/r_B is much higher than that observed in the transformation from the pyrochlore-type to the fluorite-type phase in the $Ln_2Zr_2O_7$ system. Therefore a part from cation radius ratio consideration, the structural transformation in the present system may be attributed to the crystal chemistry of the cations substituted at the A (Ca^{2+} for Y^{3+}) and B (Ta^{5+} for $Zr^{4+)}$ sites.

West et al. [45] synthesized and characterized one known, and three new pyrochlore solid solutions. PND studies show a distribution of the oxygen between the 8b and 48f sites for $Y_2TiNbO_{6.76}$, and half occupancy of the 8a site for $Y_2TiNbO_{7.5}$. In addition, the data for this Nb-based compound are consistent with both a standard pyrochlore model, and a B-site displacement model in which the B-site cations displace off of their special positions. TGA and magnetic studies suggest some preference for a $Ti^{3+/}M^{5+}$ combination in these solid solutions, rather than a purely $Ti^{4+/}M^{4+}$ combination on the B-site. Moreover, the loss of magnetism after the low temperature oxidation, shown to be Ti^{3+} oxidation, indicates Ti^{3+} as the source of local moments in these compounds. This conclusion is further supported by the increase in the peff/f.u. with the

increase in Ti^{3+} content for the Ti only and Ti/Ta-based compounds. These results indicate that the pyrochlore family of niobates, unlike the crystallographic shear structures, does not support the existence of local moment magnetism for Nb^{4+}.

Weiguang et al. [46] were successfully synthesized Ultrafine $Ln_2Ti_2O_7$ (Ln=Sm, Gd, Dy, Er) crystals at~700–800°C by the stearic acid method. The products obtained are of quadrilateral like and the average particle size is about 40 nm; the BET surface area is ca. 12m2/g. The atomic structure of Ln has a minor effect on the crystal structure of $Ln_2Ti_2O_7$. Every X-ray diffraction peak of $Ln_2Ti_2O_7$ shifted to a slightly higher angle with increasing atomic number from Sm to Er, which suggests a decrease in the lattice constant a. Also, the interplanar distance of (111) decreased with the decrease in ionic radius from Sm^{3+} to Er^{3+}. These two results are quite consistent with each other and the decrease in the ionic radius of Ln^{3+} may result in the decrease in the lattice constant. This research offers a simple and fast synthetic route for fabricating ultrafine $Ln_2Ti_2O_7$ (Ln=Sm, Gd, Dy, Er) pyrochlore oxides at lower temperatures and shortened reaction time.

Chapter-3 Characterization Techniques

This chapter introduces the experimental techniques and procedure in detail for sample preparation. Samples are characterized using x-ray diffraction, Scanning electron microscopy, thermal analysis and conductivity measurement technique. The XRD technique is used to detect the formation of pyrochlore phase at room temperature whereas DTA/TGA is used to detect phase transition in samples. SEM analysis of sample is carried out to reveal the micro structural feature of saample. Conductivity of sample measured by impedance spectroscopy technique.

3.1 Sample preparation

Chemicals TiO_2 (99.99% purity), Ti_2O_3 (99.99% purity sigma Aldrich) and Y_2O_3 (99.99% purity) in powder form were taken as starting material. Sample YTi is formed by taking TiO_2 and Y_2O_3 in 1:1/2 ratio, and sample YTi2 form by taking Ti_2O_3 and Y_2O_3 in 1:1/2 ratio. A high energy ball Mill Retsch PM100 is used. The sample YTi milled in air at room temperature for 1, 5, 10, 20, and 40h respectively at room temperature with 450 rpm. Ball weight to material weight ratio is kept 10:1. After each milling time interval we take 5 gm of powder mixture and characterize the powder.

3.1.1 Pellet Preparation

The known weight 40 h ball milled powder of YTi and YTi2 was transferred in die of 20 mm. The die along with punch was kept below hydraulic press and compaction pressure of 10 ton was applied slowly. After waiting 1 minute, the pressure was released and compact mass was ejected out.

3.1.2 Sintering

In the present work we made the two series of samples, one is single sintered and other is double sintered. Two pellets of YTi and YTi2 obtained after compaction were sintered at 1450°C for 12 h in a calibrated high temperature resistance furnace. And other two pellets of YTi and YTi2 were double sintered at 800°C and 1000°C for 12h respectively to optimize the processing condition for achieving better properties.

3.2 X-ray Diffraction

X-ray diffraction (XRD) is a versatile, non-destructive technique used for qualitative and quantitative analysis of a crystalline materials. This experimental technique has been used to determine the overall structure of bulk solids, including lattice constants, identification of unknown materials, orientation of single crystals, orientation of polycrystalline, stress, texture, films thickness etc. In this study a powder diffraction system with Cu-Kα x-ray tube (λ=1.54 A^0) was used. The x-ray scans were performed between 2θ values of 30° and 80° with a typical step size of about 0.1° [47].

3.2.1 Bragg's Law

Since atoms are arranged periodically in a lattice, x-rays scattered from a crystalline solid can constructively interfere, producing a diffracted beam through these atoms. In 1912, W. L. Bragg recognized a predictable relationship among several factors. These factors are combined in Bragg's law:

$$n\lambda = 2d \sin \theta \qquad (1)$$

n = an interger-1, 2, 3….etc [n=1 for our calculations]

λ = the wavelength of the incident X-radiation, symbolized by the Greek letter lambda and, in this case, equal to 1.54 angstroms. d = the distance between similar atomic planes (interatomic spacing) which we call the d-spacing and measure in angstroms.

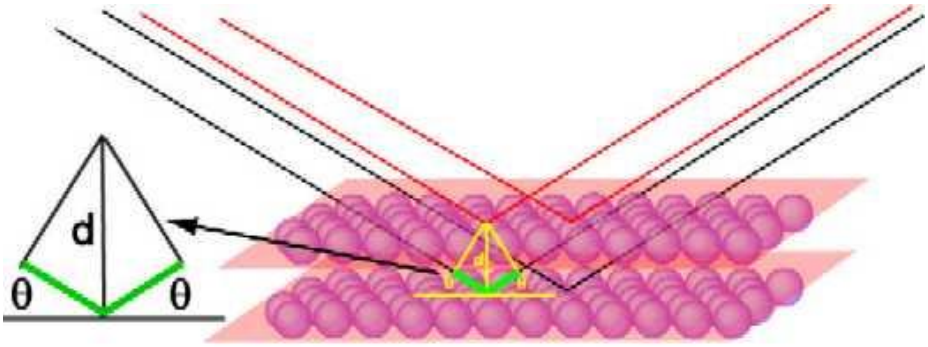

Figure 3.1: Bragg's diffraction condition.

3.2.2 Determination of lattice parameters

For the pyrochlore structure the interplanar distance of (hkl) plane is related to the lattice parameters a, the Miller indices hkl:

$$d=a/(h^2+k^2+l^2)^{1/2} \qquad (2)$$

For the lattice parameters determination for a c-plane oriented film includes a measurement of d_{100} in order to determine the c lattice parameter, and for the determination of a lattice from a second measurement of with either h or k different from zero.

3.2.3 Crystallite size measurement

Phase identification using x-ray diffraction depends on the positions of the peaks in a diffraction

profile as well as the relative intensities of these peaks to some extent. Another aspect of the Diffraction from material is the importance to consider how diffraction peaks are changed by the presence of various types of defects such as small number of dislocations in crystals with dimensions of millimeters. Small size of grain size can be considered as another kind of defect and can change diffraction peak widths. Very small crystals cause peak broadening. The crystal size is easily calculated as a function of peak width (specified as the full-width at half maximum peak intensity (FWHM)), peak position and wavelength.

3.3 Scanning Electron Microscopy (SEM)

The SEM is a very important and powerful analysis tool for imaging structures ranging from the millimeter to the nanometer scale [48]. Due to the extremely small wavelength of the highly accelerated electrons, the SEM can resolve features down to the nanometer regime. The interaction between the electron beam and the sample surface, gives rise to different particles and waves, carrying information about the sample, as shown in Fig 3.2(a-c). For example, Auger electrons and X-rays carry characteristic energy and can be used for element identification, secondary electron intensity provides topographical information, whereas back scattered electron enable material with different atomic number to be distinguished.Scanning electron microscopy (SEM) is basically a type of electron microscope. SEM is used for various purposes;

- Topographic studies.
- Microstructure analysis.
- Elemental analysis if equipped with appropriate detector (energy/wavelength dispersive x-rays).
- Chemical composition.

- Elemental mapping.

In SEM, Primary electrons are thermonically or field emitted by a cathode filament (W or LaB_6) or a field emission gun (W-tip) and after that accelerated with high energy typically 1-30KeV. The electron beam is steered with scanning coils over the area of the interest. Upon interaction with material, the primary electrons decelerate as well as losing his energy, transfer it inelastically to other atomic electron and to the lattice. Due to continuous scattering events the primary beam spread up with different energies depending on source origin as shown in figure. 3.2.(a.) the interaction volume with the various electrons emitted and their respective energy is shown in figure 3.2.(b).

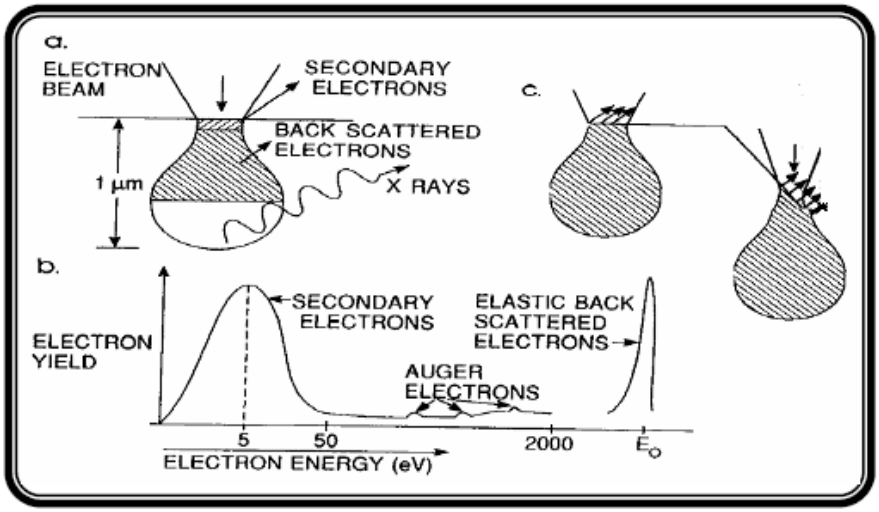

Figure3.2.(a) Electron interactions with the surface during bombardment. (b) Type of electrons and corresponding energies of the emitted electrons after element interaction. (c) Effect of surface topography on electron emission.

Secondary electrons (1-50eV) are mostly used for the imaging the topographically contrast and reproduce the surface. High energy elastically backscattered electrons depends on the atomic number (Z) of the element, which is useful to obtain Z-contrast. X-ray characteristic can be used to qualitatively and quantitatively analyze the elemental composition and distribution in the sample.

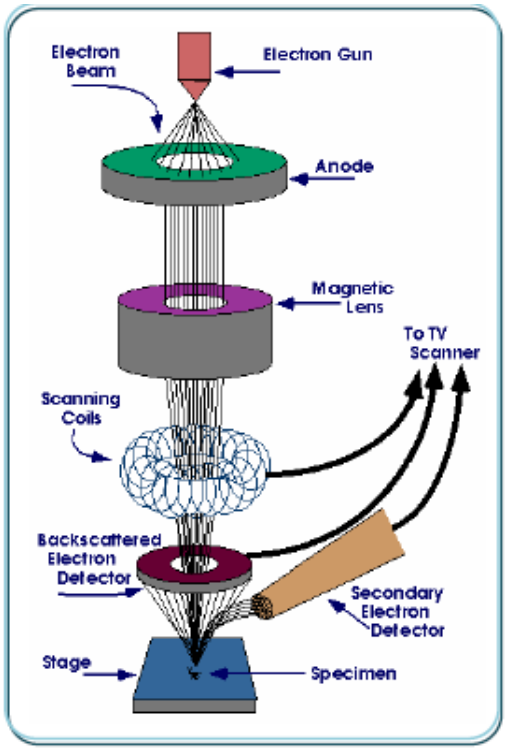

Figure 3.2.(d): Schematic illustration of the SEM.

3.4 Thermo Gravimetric Analysis

Thermo gravimetric Analysis (TGA) is a type of testing that is performed on samples to determine changes in weight in relation to change in temperature. Such analysis relies on a high degree of precision in three measurements: weight, temperature, and temperature change. As

many weight loss curves look similar, the weight loss curve may require transformation before results may be interpreted. A derivative weight loss curve can be used to tell the point at which weight loss is most apparent. Again, interpretation is limited without further modifications and deconvolution of the overlapping peaks may be required.

TGA is commonly employed in research and testing to determine characteristics of materials such as polymers, to determine degradation temperatures, absorbed moisture content of materials, the level of inorganic and organic components in materials, decomposition points of explosives, and solvent residues. It is also often used to estimate the corrosion kinetics in high temperature oxidation. The analyzer usually consists of a high-precision balance with a pan (generally platinum) loaded with the sample. The pan is placed in a small electrically heated oven with a thermocouple to accurately measure the temperature. The atmosphere may be purged with an inert gas to prevent oxidation or other undesired reactions. A computer is used to control the instrument. Analysis is carried out by raising the temperature gradually and plotting weight against temperature. The temperature in many testing methods routinely reaches 1000°C or greater, but the oven is so greatly insulated that an operator would not be aware of any change in temperature even if standing directly in front of the device. After the data is obtained, curve smoothing and other operations may be done such as to find the exact points of inflection to analyze the composition.

3.5 Differential Thermal Analysis (DTA)

Differential thermal analysis (DTA) is a thermo analytic technique, similar to differential scanning calorimeter. In DTA, the material under study and an inert reference are heated (or cooled) under identical conditions, while recording any temperature difference between

sample and reference. This differential temperature is then plotted against time, or against temperature (DTA curve). Changes in the sample, either exothermic or endothermic, can be detected relative to the inert reference. Thus, a DTA curve provides data on The transformation occurred at glass transition, crystallization and melting .In the present work differential thermal analysis of the powdered samples will be done by DTA, Perking Elmer (Diamond TG/DTA) in nitrogen atmosphere, using platinum crucibles at 10˚C/min heating rates from room temperature to 1000^{o}C. The reference sample taken was α-alumina. Thermographs have been taken between temperature and endothermic, showing the transition and melting of the samples.

3.7 Ionic conductivity

As is evident from the previous discussions the factors that influence the conductivity in the solid state are the concentration of charge carriers, temperature of the crystal, the availability of vacant-accessible sites which is controlled by the density of defects in the crystal and the ease with which an ion can jump to another site etc. The last of the above discussed factors, namely, the ease with which an ion can jump to a neighboring site is controlled by the activation energy. The 'activation energy' is a phenomenological quantity. It may be said to indicate the free energy barrier an ion has to overcome for a successful jump between the sites. Among the various factors that influence the ionic conductivity of a crystal the activation energy is of utmost importance since the dependence is exponential. It can be measured quiet conveniently by experiments. The activation energies are most commonly deduced using the Arrhenius expression, given by,

$$\sigma = (A/T) \exp (-Ea/K_B T) \qquad \text{……..…….(1)}$$

where σ is the conductivity at temperature T in K, k_B is the Boltzmann's constant, Ea is the activation energy and A is called the pre-exponential factor. The pre-exponential factor, A, contains all the remaining factors, i.e., other than the activation energy, that influence the ionic conductivity. The activation energy, Ea, may be deduced easily from the slope of the ln(σ T) versus T^{-1} plot. The random walk theory supports the above functional form of s and also describes A in terms of other factors that influence the ionic conduction.

The Nernst–Einstein expression relates the ionic conductivity to the diffusion coefficient of ions and is particularly useful in molecular dynamics study. The Nernst–Einstein expression suggest that the conductivity,

$$\sigma = nq2D/k_BT \qquad \text{……..……..……} \quad (2)$$

where n is the number of ions per unit volume, q is its charge and D the self-diffusion coefficient of ions,

$$D = zNc(1 - c)al2n/k_BT, \qquad \text{……..(3)}$$

where z is the number of nearest neighbor sites of density N, c is the concentration of ions, al the distance between the sites and n is the jump frequency given by,

$$n = n_0 \exp(-Ea/k_BT), \qquad \text{……. (4)}$$

where Ea is the free energy barrier associated with the ion hop between two sites and n0 is the cage frequency (site frequency) of the ion. The expression suggest that for high diffusivity in solids,

(1) High density of mobile ions (c),

(2) The availability of vacant sites (that can be accessed by the mobile ions) (1 – c),

(3) Good connectivity among the sites (requiring conduction channels with low free energy (Ea) barriers between the sites).

Chapter-4 Result and Discussion

This chapter introduces the result of prepared samples and discusses the effect of sintering temperature on structural, conducting and thermal properties of pyrochore phase $Y_2Ti_2O_7$.

4.1 XRD Analysis

Figure 4.1(a) and 4.1(b) shows the X-ray diffraction pattern of single sintered YTi and YTi2 at 1450 °C and double sintered YTi and YTi2 samples respectively. In fig. 4.1(a), X-ray of single sintered YTi depicted that single phase of pyrochlore ($Y_2Ti_2O_7$) is present after heat treatment. This phase is indexed with ICDD card number [73-1697]. Peaks are sharp and well resolved each other. Density of YTi sample is 84% of theoretical density X-ray of sample YTi2 result in the formation of double phase. One is pyrochlore $Y_2Ti_2O_7$ phase and other is unreacted TiO_2 phase. This TiO_2 phase is index with ICDD card number [75-6234]. Volume fraction of $Y_2Ti_2O_7$ and TiO2 is 92% and 8% respectively in single sintered YTi2 sample. Second phase TiO_2 is present due to conversion of Ti^{+3} to Ti^{+4}. The density of YTi2 sample is 97% of theoretical density. The sintered sample shows the contraction in lattice parameter in both the sample. As

reported earlier that during heat treatment process some Y^{3+} and Ti^{4+} ions occupy the sites interchangeable in pyrochlore symmetry and their redistribution follows ordered pyrochlore [49]. Figure 4.1(b) shows the XRD pattern of double sintered YTi and YTi2. Double sintered YTi containing again single pyrochlore phase but density decrease in comparison than single sintered YTi sample. Double sintered YTi2 also show the presence of pyrochlore $Y_2Ti_2O_7$ and unreacted TiO_2. In this phase volume fraction of TiO_2 phase is 25% which is more than single sintered YTi2. Density of double sintered sample decrease comparison of single sintered YTi2. In double sintered YTi2 sample sintering temperature are 800°C and 1000°C for 12h, but conversion of Ti^{+3} into Ti^{+4} takes at high sintering temperature, so some concentration of Ti^{+4} result in formation of pyrochlore phase and about 25 weight percentage of TiO_2 remains unreacted.

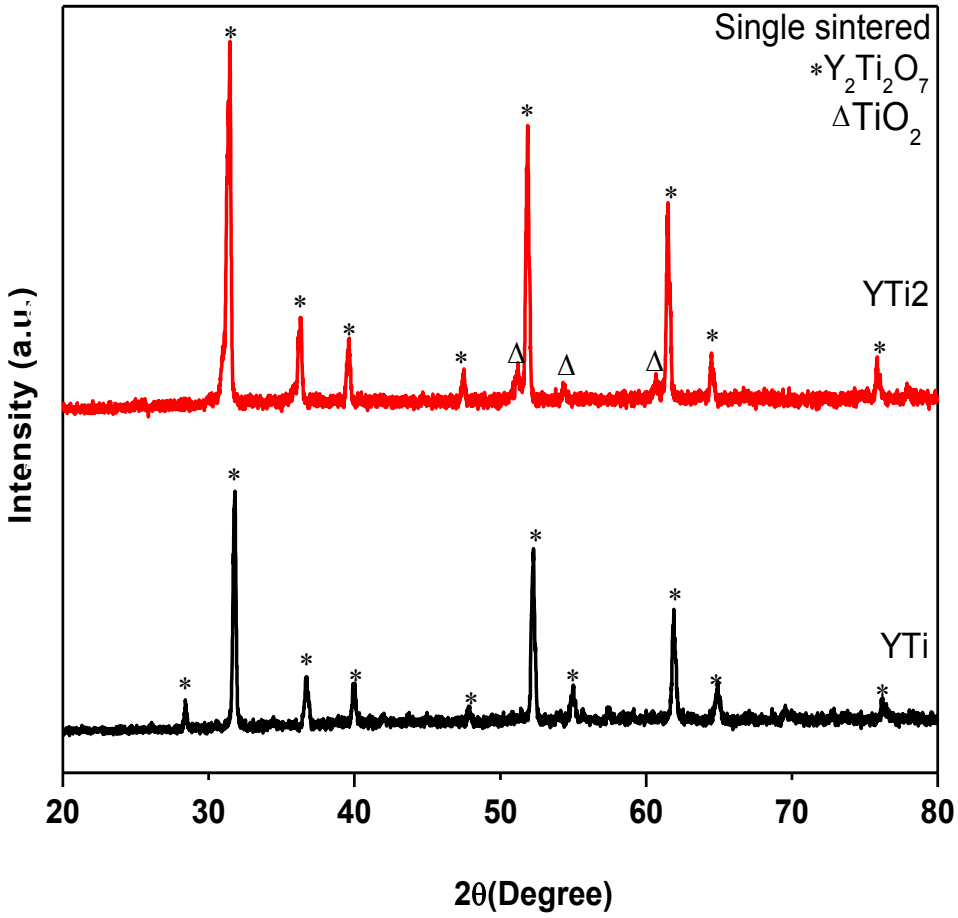

Figure: 4.1(a)-XRD pattern of single sintered YTi and YTi2.

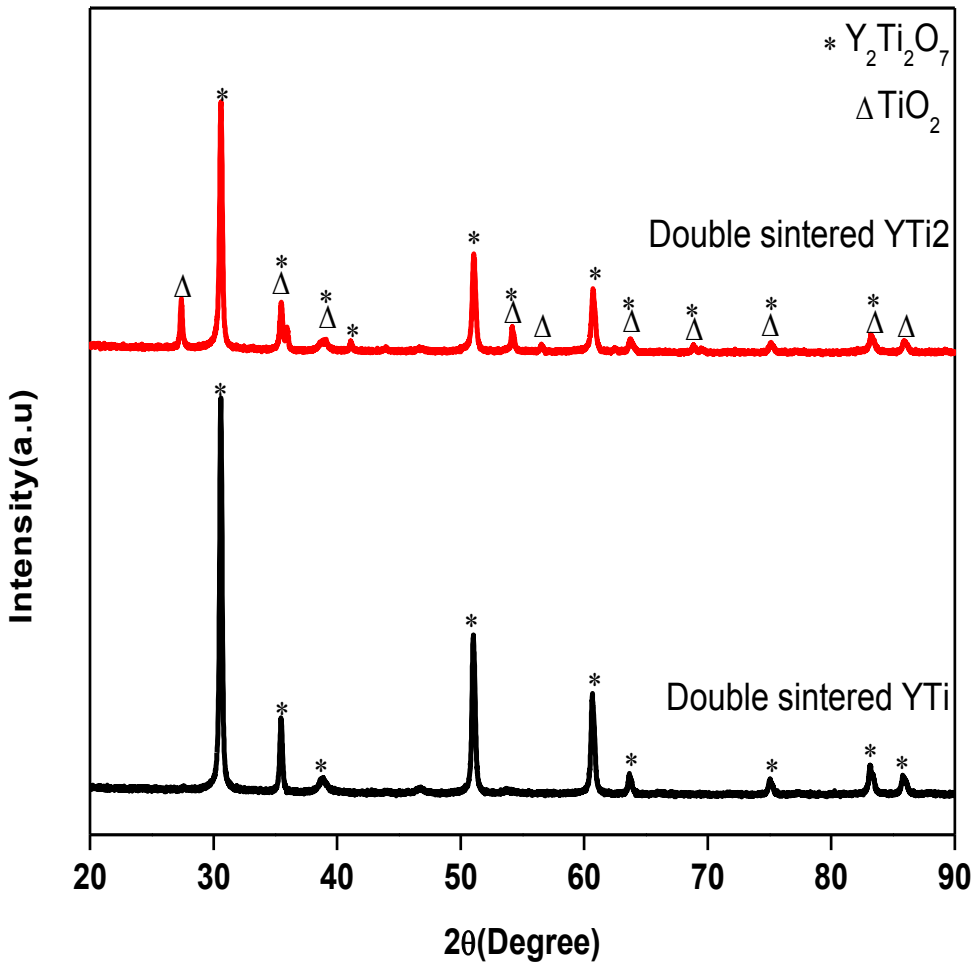

Figure: 4.1(b)-XRD pattern of double sintered YTi and YTi2.

4.2 SEM analysis

The typical micrographs of single sintered and double sintered samples are shown in figure 4.2(a) and 4.2(b), respectively. From fig.4.2 (a), single sintered sample YTi micrograph shows the fracture surface of pellet. There is no resolved grain boundary. Non uniform distribution of grains and porosity is continuous. From SEM image of YTi2, we observed there is uniform distribution of grains and well resolved grain boundary. In figure 4.2(b) As observed in

micrographs, the particles are agglomerated and irregular in shape with variable grain size. It is common phenomena in ball milled sample. The larger agglomeration is found in Double sintered YTi2 sample as compared to double sintered YTi sample. Unfortunately, the estimation of particle size is difficult in the present samples due to agglomeration and lower magnification. Earlier ball milling duration, the plastic deformation and cold welding are taken place, which cause agglomeration of particles. The variation of particle size and agglomeration is mainly due to different mechanism for grinding particle at the different ball milling condition [50]. The grain size evaluated from the micrograph is in the range of 1 μm. It was found that the grains were homogenously and uniformly distributed over the entire surface of the sample.

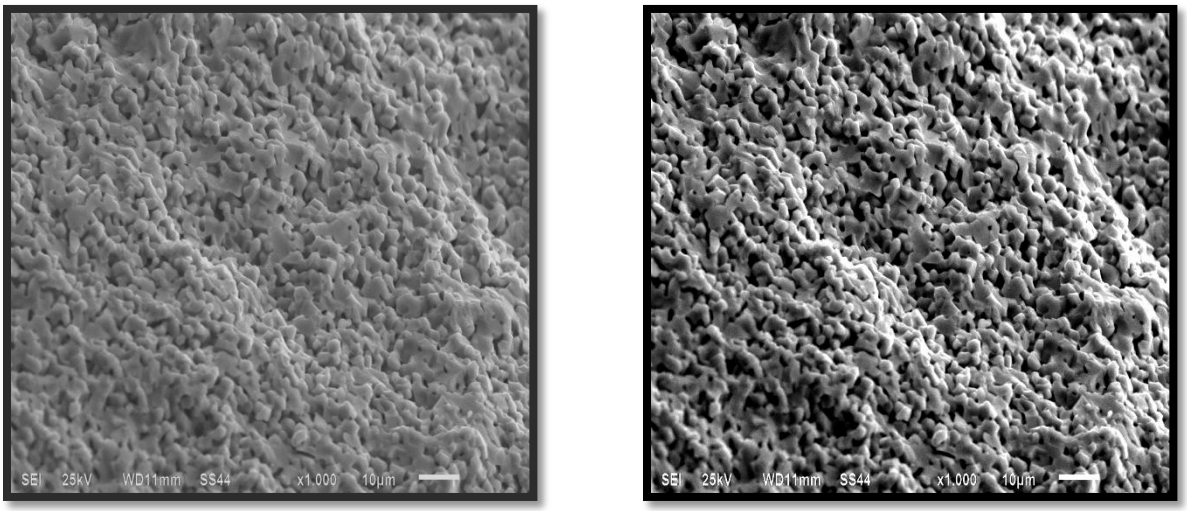

(YTi) (YTi2)

Figure 4.2(a): SEM image of single sintered sample

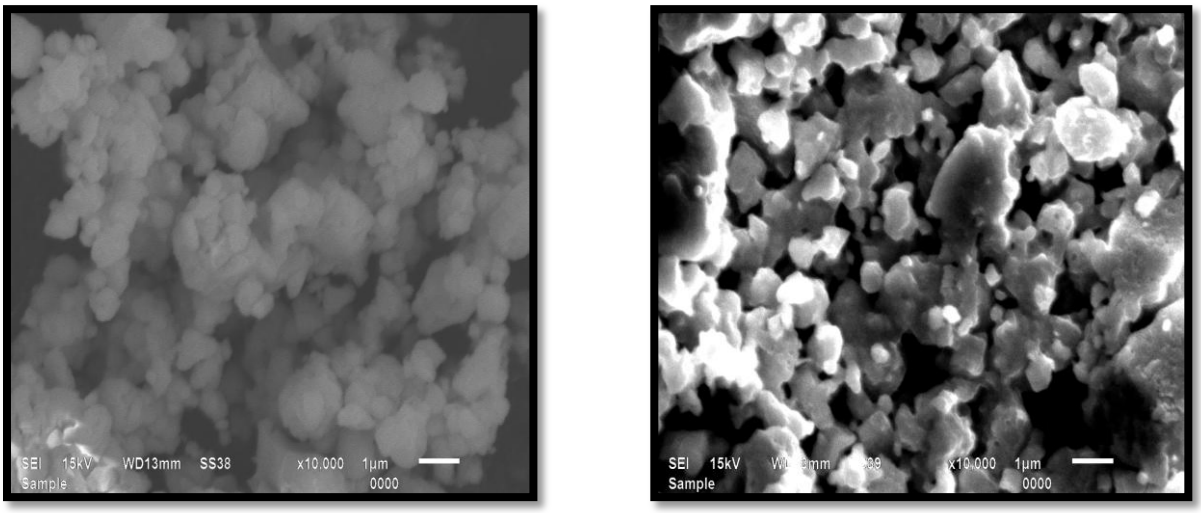

(YTi) (YTi2)

Figure 4.2(b): SEM image of double sintered YTi2 sample.

4.3 Electrical Conductivity study

The conductivity of samples is shown in figure 4.3(a) and 4.3(b). The total resistance of sample was calculated from the point of intersection of cole-cole semicircle plot at the real axis. The conductivity was calculated using the following formula:

$$\sigma = \frac{l}{RA} \qquad \text{.....(1)}$$

Where l is the thickness of the pellet and A is cross section area of the pellet. As temperature increasing the resistance of sample drops, this is manifestation of high temperature ionic conduction. In other words, the conductivity in $Y_2Ti_2O_7$ phase should be arised due to thermally activated hopping conduction of the oxide ions in oxidizing atmosphere. The present sample

clearly shows two linear regions. The activation energies of both regions are calculated by linear square fitting of Arrhenius plots. The activation energy along with conductivity is given in table 1. The activation energy of single sintered YTi sample is slightly higher than YTi2. It is also observed that the conductivity (3.34 $x10^{-6}$ S/cm) of YTi2 sample is one order higher than YTi (7.63 $x10^{-7}$ S/cm). The higher conductivity might be attributed due to presence of Ti^{3+}/Ti^{4+} mixed state in this sample. The mixed state of B ions may cause higher disordering in the system and is responsible for higher ionic conductivity. Figure 4.3(b) shows the combined conductivity graph of double sintered YTi and YTi2. The activation energies of both samples are calculated by linear square fitting of Arrhenius plots. The activation energy along with conductivity is given in table 1. From the study of activation energy and conductivity value we observed that very low energy is required for movement of ion due to low density of double sintered sample with respective to standard density. Conductivity of both samples is observed $2.99x10^{-4}$ S/cm. It is observed that the magnitude of Z' decreases with the increase in both frequency as well as temperature indicating an increase in a.c. conductivity with the rise in temperature and frequency. The values of Z' for all temperatures merge above 10 kHz. This may be due to the release of space charges as a result of reduction in the barrier properties of material with the rise in temperature, and may be a responsible factor for the enhancement of a.c. conductivity of material with temperature at higher frequencies.

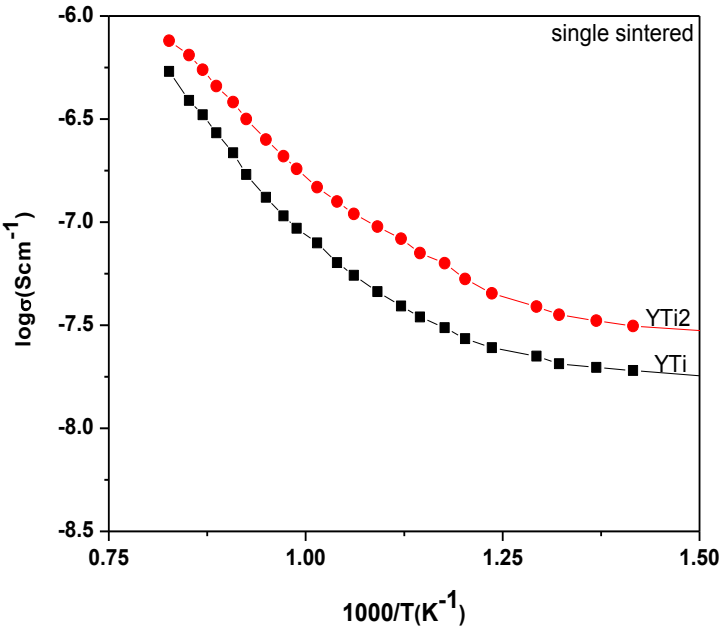

Figure-4.3(a): Combined Arrhenius plot of single sintered YTi and YTi2.

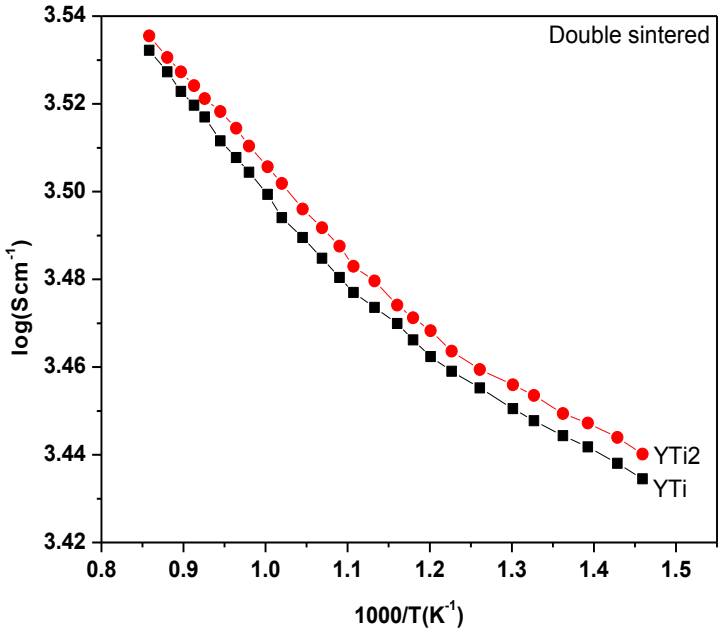

Figure-4.3(b): Combined Arrhenius plot of double sintered YTi and YTi2.

4.4 Thermal analysis

Figure 4.4(a) shows the DTA of single sintered YTi and YTi2 respectively. During heat treatment, rearrangement and redistribution of cations and oxygen ions take place in ball milled samples. Density of single sintered sample is nearly to theoretical density so energy slightly vary with temperature. This process convert ball milled sample in to ordered pyrochlore systems. In fig. 4.4(a) exothermic peaks are observed after 800°C. This peak reports convession of disordered pyrochlore to ordered pyrochlorre [24]. Figure 4.4(b) shows the DTA of double sintered YTi and YTi2 samples respectively. There is sharp energy loss in both samples because density is very low comparable to theoretical density. As temperature is increased atoms are reoriented, due to low density reorientation process become fast and energy loss is high with temperature.

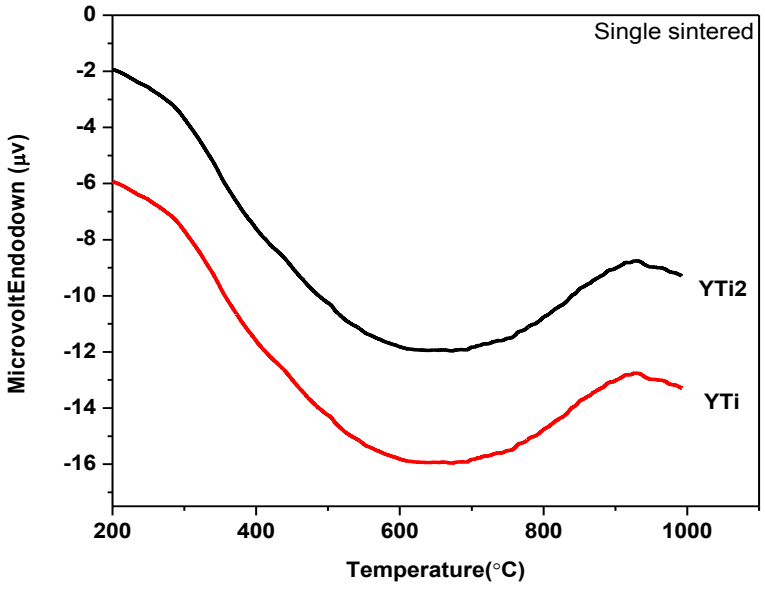

Figure 4.4(a): Combined DTA of single sintered YTi and YTi2.

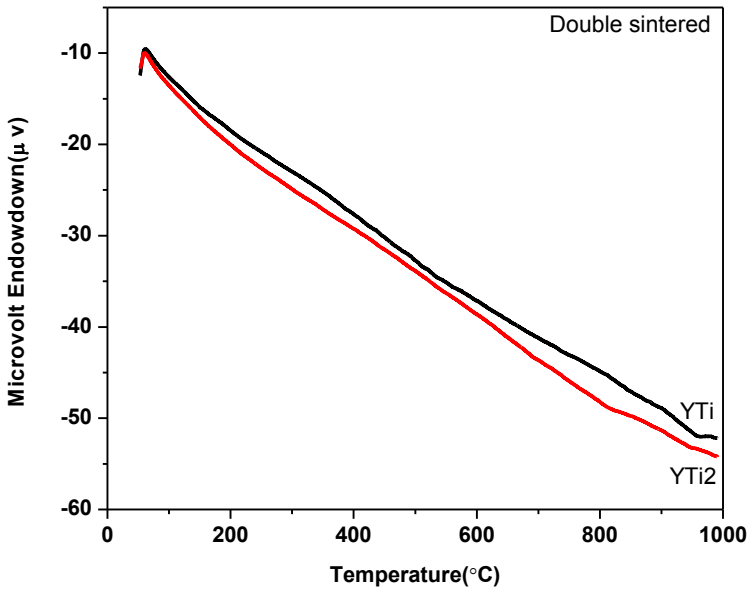

Figure 4.4(b): Combined DTA of double sintered YTi and YTi2.

4.5 Particle size analysis

Figure 4.5(a) and 4.5(b) shows the variation in particle size with ball milling time of double sintered YTi and YTi2 sample. From fig. 4.5(a), Yttrium oxideY_2O_3 is hydrophilic and TiO_2 is hydrophobic in nature. After 1 hour of ball milling particle size is found to be 216.5 nm. Balls have an impact on each other so plastic deformation and cold welding is taking place inside the vial. Further 5 hours ball milling causes cold welding because thermal energy produces heat. Particle size decreases due to cold welding mechanism and reached 155.5nm. Further 5 hours of ball milling, result in the formation of pyrochlore phase and some crystal lattice energy is released. So particle size increases and reached 254.2 nm up to 10 hours ball milling. After 10 hours ball milling particle size decreases due to compression in lattice parameter after releasing energy. After 20 hours ball milling larger amount of thermal energy transfer to the material. There is reorientation of atoms so particle size increase upto 40 hours ball milling. From fig.4.5

(b), sample YTi2 is stiochiometric mixing of Y_2O_3 and Ti_2O_3. Y_2O_3 and Ti_2O_3 both are hydrophilic in nature. After 1 hours ball milling, particle size is 523.2nm. After 5 hour of ball milling, some heat is arising which make strong bonding in constituents component subsequently powder become adhesive and particle size increases and reaches 674.2nm. Further 5 hour of ball milling, no significant transformation in particle size. After 10 hours of ball milling, there is no new phase formation so due to cold welding mechanism adhesion of powder increases. Particle size increases and reaches 730.3nm. Further during 10 hours of ball milling, pyrochlore phase formed. During phase formation crystal energy is released which makes the powder hydrophobic and plastic deformation mechanism taken place. So after 20 hours ball milling particle size decreases and found to be 610.5 nm. Further 20 hours of ball milling, more impact of balls on powder produce more heat which makes the powder hydrophobic. There is no compression force among the particles and particles are dispersed. Particle size decreases and reaches 426.5 nm as shown in figure 4.5(b).

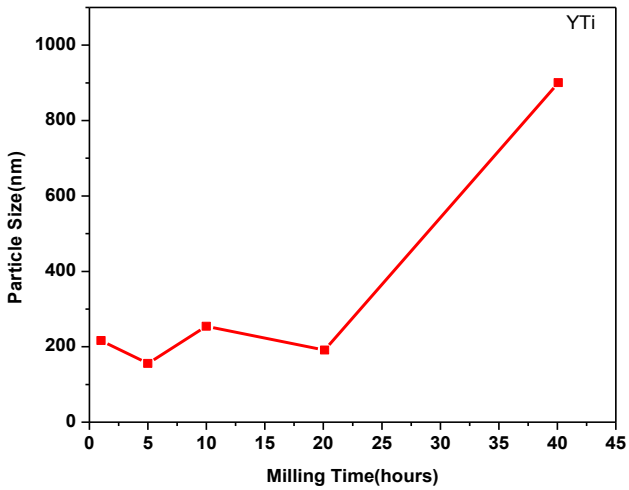

Figure 4.5(a). Particle size vs. Ball milling time.

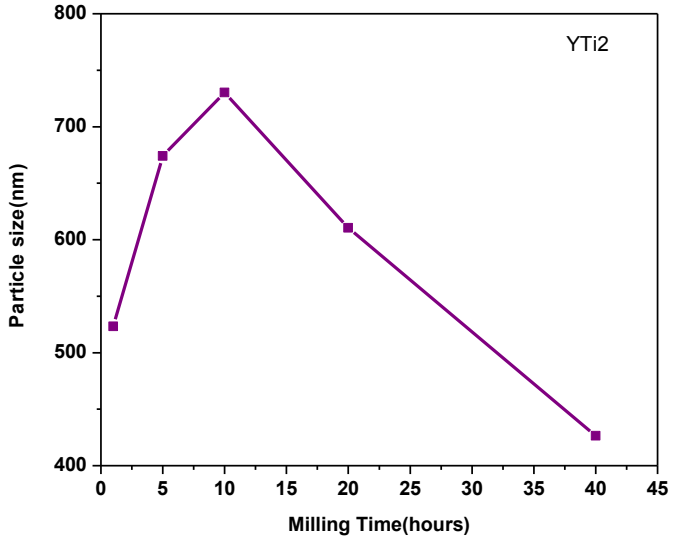

Figure 4.5(b). Particle size vs. Ball milling time.

Table-1: This shows the activation energy, thermal expansion coefficient and conductivity.

Sample name	Temperature Range(°C)	Activation energy (eV)	Thermal Expansion Coefficient($x10^{-6}$)	Conductivity S/cm^{-1}
Single sintered YTi	T > 660	0.61	8.389	$1.95x10^{-6}$
Single sintered YTi2	T > 680	0.59	8.212	$2.23x10^{-7}$
Double sintered YTi	T > 660	0.17	8.343	$2.99x10^{-4}$
Double sintered YTi2	T > 680	0.18	8.405	$2.98x10^{-4}$

Table-2: This shows Density and lattice parameter of single and double sintered sample.

sample	Experimental density(gm/cc)	Relative density (%)	Lattice parameter(Å)
Single sintered YTi	3.88	84.3	9.90
Single sintered YTi2	4.81	97.1	9.97
Double sintered YTi	1.87	40	10.15
Double sintered YTi2	2.80	62	10.02

Chapter-5 Future Work

The challenges of meeting rapidly growing demand for cleaner energy will require developing new high-temperature, high-performance ceramics with outstanding properties that are sustained under long-term service in severe environments. . Ionic conduction in ceramics has become a major field of research. As society searches for alternatives to fossil fuels, many have turned to hydrogen as an alternate. Recently different pyrochlore materials are synthesized by different routes. A very few reports are appeared in the literature where pyrochlore have been synthesized by thermo mechanical route. As mention in the literature, higher disordering can be in corporate in pyrochlore structured material which may lead to higher ionic conductivity at lower temperature. The high ionic conductivity materials can be used as a solid electrolyte in solid oxide fuel cells. Solid Oxide Fuel Cells (SOFC) take advantage of converting chemical energy directly to electrical energy, which offers a clean and abundant source of fuel. To further improve the efficiency of SOFCs, a detailed understanding of the mechanism of ionic conduction is necessary. On the other hand, the Yittria Stabilized Zirconia (YSZ) electrolyte generally operated at about 1000˚C, where ionic conductivity reaches the required high level. However such high temperature needs high fabrication cost and degradation of cell components. To reduce the operating temperature of solid oxide fuel cell (SOFC) systems, recently alternate electrolyte materials are investigated. We will continue to synthesize doped Sr and Ca samples of varying composition and thermal history, as well as ordered model compounds, to better understand the relationships between atomic structure and conducting properties. We will also continue our new work on other oxide ion conductors, such as doped bismuth and cerium oxides.

References

1. E. Aleshin , R. Roy, J Am Ceram Soc 45 (1962) 18.

2.L.Minervini, R.W.Grimes and K.E Sickafus, j.Am.ceram.Soc.83 (2000) 1873.

3.M.A. Subramanium, G.Aravamudan, G.V SubbaRao, prog.Solid Statechem.15(1983)55.

4.Kennedy, B.J, Hunter, B.A. Howard, C.J, J Solid state Chem, 58(1997)130.

5. Stanek C, R. Minervini L, Grimes RW, J Am Ceram soc 85(2002)2792.

6.C Hereman, B.J. Wuensch, J. k Stalick, E. Prince,J solid state chem.117(1995)108.

7.A web of science search (1975 to present) for articles containing the term pyrochlore in title returned 837 hits.

8.B. J. Kennedy, Physica B 303(1998)241-243.

9.L.Minervini, R.W.Grimes, K.E Sickafus, J.Am.Ceram.Soc. 83(2000)1873

10. B.J Wuensch, K.Weberman, C.Heremans, E. Prince, J. solid state chem.117(1995)108.

11. Onnerud, E. M.Yeo, S. M. Haile, J. K. Stalick, J.D. Jorgensen, Solid State,129(2000)111.

12. M. Pirazada, R.W. Grimes, J.F. Maguire, solid state ionics81(2003)161.

13. G.D. Blundered , C.A. bridges, M.J. Rosseinsky, Angew Chem.int. Ed. 43(2004) 3562.

14. B.P. Mandal, Nandini Garg, Surinder M. Shrama, A. K Tyagi. Journal of Solid State176(2006).

15. B.J Wuensch, K.Weberman, C.Heremans, E.M. ku, P. Onnerud, E .M. Yeo, S.M.Haile, J.K.stalick, J.D..Jorgensen, Solid Stat Ionics 111(2000)129.

16. Porat O, Heremans C, Tullar HL. Solid state ionics 94(1996) 751990-1994.

17. j.K. Park, C.H. Kim, K.J. Choi, j.Mater.res.16 (2001) 2568.

18. A. Digeos, J.A.Valdez, K.E.Sickafus, S. Atiq, R.W Grimes, A.R Boccaccini, J. Mater.Sci.38 (2003) 1597.

19. T.R.Malow,C.C.Koch,Acta Mater. 46(18) (1998)6459-6473.

20. W.J. Weber and R.C. Ewing, Science, 289 (2000) 2051-2052.

21. W.J. Weber, J.W. Wald and Hj. Matzke, Mater. Lett. 3(1985) 173.

22. H. Gleiter, Acta mater. 48(1)(2000)1-29.

23. C. Suryanarayana, Int. Mater. Rev. 40(2)(1995)41.

24. AntonioF. Fuentes, Khalid Boulahya, Miroslaw maczka, Jerzy hanuza, Ulisas Amadar, solid state 7(2005) 343-353.

25. M. Hanawa, J. Yamaura, Y. Muraoka, F. Sakai, Z. Hiroi, Phys. chem. Solids 63(2002)1027.

26. Zhi-Fen Fu, Peng Liu, Xiao-Ming Chen, Jian-Li Ma and Huai-Wu Zhang, Journal of Alloys and Compounds 493 (2010) 441-444.

27. J. Lian, J. Chen, L.M. Wang, R.C. Ewing, J.M. Farmer, L.A. Boatner, K.B. Helean, Phys. Rev. B 68 (2003) 134107.

28. Jin-Ho Lee, Masatomo Yashima, Masato Kakihana, and Masahiro YoshimuraJ. Am. Ceram. Soc., 81 [4] (1998) 894–900.

29. Gregory R. Lumpkin, Katherine L. Smith, Mark G. Blackford, and Karl R. Whittle Elizabeth J. Harvey and Simon A. T. Redfern Nestor J. Zaluzec Chem. Mater. 21 (2009) 2746–2754.

30. A. Michael, Hayward, Chem. Mater. 17 (2005) 670 -675.

31. K. Muthukkumaran Æ Roshan Bokalawela J Mater Sci 42 (2007) 7461–7466.

32. Shin Miyahara , Ai Murakami, Nobuo Furukawa, Journal of Molecular Structure 838 (2007) 223–226.

33. B. Z. Malkin and A. R. Zakirov, M. N. Popova, S. A. Klimin, and E. P. Chukalina, E. Antic-Fidancev, Ph. Goldner, and P. Aschehoug ,G. Dhalenne, Physical Review B 70 (2004) 075112

34. J. S. Park, Y. H. Han,K.H. Choi Journal of Material Science in Electronics 16 (2005)215–219.

35. Michel B. Johnson , David D. James a, Alex Bourque a, Hanna A. Dabkowska ,Bruce D. Gaulin , Mary Anne White, Journal of Solid State Chemistry 182 (2009) 725–729.

36. A. Chartier, C. Meis, J.-P. Crocombette, W. J. Weber, and L. R. Corrales PRL 94 (2005)025505.

37. M. Deepa, P. Prabhakar Rao , A.N. Radhakrishnan, K.S. Sibi, Peter Koshy, Materials Research Bulletin 44 (2009) 1481–1488.

38. Karl R.Whittle , Lachlan M. D. Cranswick , Simon A. T. Redfern, Ian P.Swainson , Gregory R. Lumpkin, Journal of Solid State Chemistry 182 (2009) 442–450

39. K.B. Tan, C.C. Khaw, C.K. Lee, Z. Zainal, G.C. Miles, Journal of Alloys and Compounds 508 (2010) 457–462.

40. B.P.Mandal , P.S.R.Krishna , A.K.Tyagi, Journal of Solid State Chemistry 183 (2010) 41–45.

41. Huiling Du, Xiang Shi, Yu Cui, Solid State Communications 150 (2010) 1213-1216

42. D. Jiayu , X. Yuan , H. Pengde , Z. Qitu, Journal of rare earths, Vol. 28, No. 5, Oct. 2010, p. 765

43. D.A. Belov, A.V. Shlyakhtina, S.Yu. Stefanovich , I.V. Kolbanev, Yu.A. Belousov,O.K. Karyagina, L.G. Shcherbakova, Materials Research Bulletin 44 (2009) 1613–1620.

44. A.N. Radhakrishnan, P. PrabhakarRao, K. S .Sibi, M. Deepa, Peter Koshy Journal of Solid State Chemistry 182 (2009) 2312–2318.

45. D.V. West, T.M. McQueen, Q. Huang, R.J. Cava, Journal of Solid State Chemistry 181 (2008) 1753– 1758.

46. Weiguang Zhang, Lili Zhang, Hui Zhong, Lude Lu, Xujie Yang, Xin Wang, Material characterization 6 1 (2 0 1 0) 1 5 4 – 1 5 8.

47. B.D. Cullity Elements of X-ray Diffraction Addison Wesley Mass.

48. O. C. Wells, Scanning Electron Microscopy, McGraw-Hill Book Company, New York.

49. Zhi-fen Fu, Peng Liu, Xiao-Ming Chen, Jian Ma, Huai-wu Zhang, J. Alloys. Compd. 493(2010) 441-444.

50. S. Ananta, R. Brydson, N.W. Thomas, J. Eur. Ceram. Soc., 19 (1999) 355-362.